Rationally stabilized hierarchical NiCo$_2$O$_4$ hollow nanoballs for high-performance asymmetric supercapacitor and excellent methanol oxidation

Vikas Sharma[a]*, Rahul Vijay Khose[b], Kushal Singh[c]

[a]Centre for Converging Technologies, University of Rajasthan, Jaipur-302004, Rajasthan, India.

[b]Mettler Toledo India, Mumbai-400072, Maharashtra, India

[c]Department of Materials Science and Engineering, NIT Hamirpur, Hamirpur-177005, Himachal Pradesh, India

Email: *vikas2008.123@gmail.com

Mathematics behind the supercapacitor performance evaluation

The specific capacitance from the CV profiles in the three electrode configuration was calculated using the relation[1]:

$$C_S = \frac{1}{2mVs} \int_{-V}^{+V} I.dV \qquad \text{(S1)}$$

where C_s, I, m, V, s represent the specific capacitance in F g^{-1}, the current generated at a certain potential in ampere (A), the mass of the active material in gram (g), potential window in volts (V) and scan rate in V s^{-1}, respectively. The voltammetric charge (q*) from the CV profiles was obtained using the undermentioned relation[1]:

$$q^* = \frac{\int I.dE}{A.V} \qquad \text{(S2)}$$

where, V, i, E and A denote the scan rate, voltammetric current (mA), potential (mV) and geometric area of the electrode (cm^2), respectively. In addition, q* can also be calculated by using the relation[1]:

$$q^* = q_0 + kV^{-1} \qquad \text{(S3)}$$

where, q_0 is the charge contribution by double layer. This approach can also be employed to extract information pertaining to the relative surface area of the coated portion on the electrode

On the other hand, the specific capacitance from the charge discharge profiles was calculated using[1]:

$$C = \frac{I.dt}{m.dV}$$

(S4)

where I/m, dt and dV denote current density in A g^{-1}, discharge time in seconds (s) and potential window in volts (V), respectively. For the device relation calculations, charge discharge curves were considered and the same relation mention in eq. S2 was utilized.

The asymmetric supercapacitor was fabricated by balancing the charge to mass ratio for both the negative and positive electrodes using the relation[2]:

$$\frac{m_+}{m_-} = \frac{\Delta V_- C_-}{\Delta V_+ C_+}$$

(S5)

where C_- and C_+ are the specific capacitances (in F g^{-1}) measured at the same scan rate, using the three electrode system, for negative and positive electrodes, respectively while ΔV_+ and ΔV_- denote the working potential window for the positive and negative electrodes, respectively.

The energy and power density of the fabricated asymmetric supercapacitor were calculated as per the relations mentioned below[2]:

$$E = \frac{1}{2 * 3.6} CV^2$$

(S6)

$$P = \frac{E}{T} * 3600$$

(S7)

where E, P, C, V, T represent energy density in Wh kg^{-1}, power density W kg^{-1}, capacitance of device in F g^{-1}, voltage window in volts (V) and discharge time of device in seconds (s), respectively.
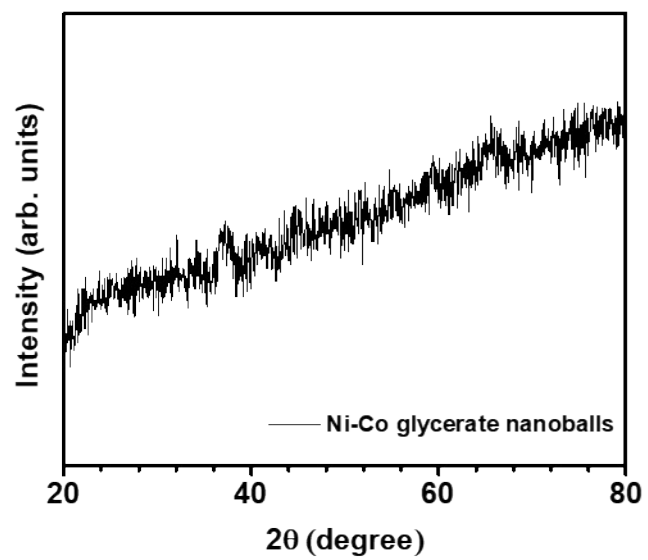
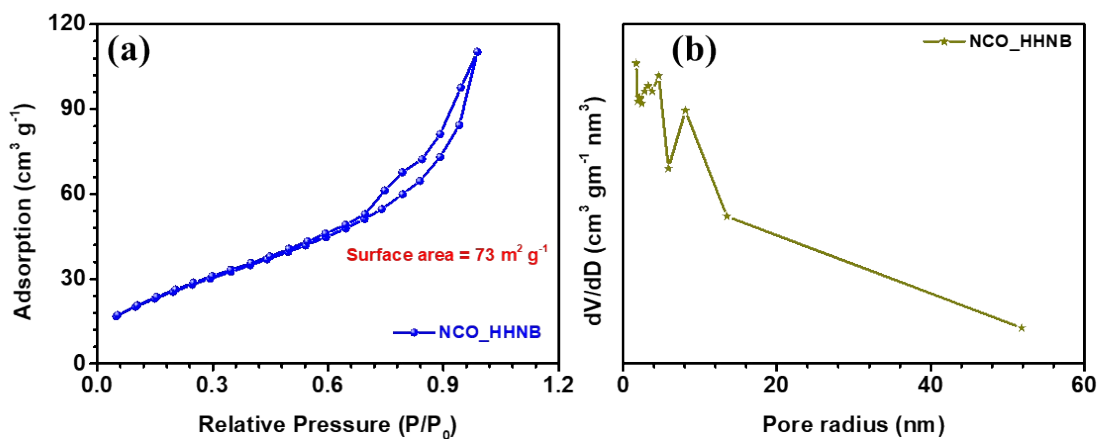**Figure S1** XRD profile of Ni-Co glycerate precursor nanoballs.

Figure S2(a) N_2 adsorption desorption isotherm and (b) pore size distribution for NCO_HHNB.

With the confirmation of the perfect hollow morphology of NCO_HHNB, the BET specific surface area and porosity calculation becomes the last critical component of material's characterization. The N_2 adsorption desorption isotherm for NCO_HHNB is shown in Fig. S2a. The calculated specific surface area was found to be ~73 m^2 g^{-1}. The higher surface area could be due to the large volumetric space of the cavity and porous external surface which provides more accommodation of gas molecules over and inside the structures internal space. The large specific surface area also increases the contact area which would consecutively increase the number of utilizable active surface sites. The amount of dead volume for the material get significantly decreased, which could enhance the electrochemical characteristics of the fabricated electrodes out of them. The shape of the isotherm represented the type IV type typical characteristic with Barrett–Joyner–Halenda pore

size (diameter) of ~4 nm, as evaluated. This confirmed the mesoporous nature of the pores present in the material. If one carefully looks at the pore radius profile then it was confirmed that all pores like in the range 2-50 nm, which is observed for perfect mesoporous structures.
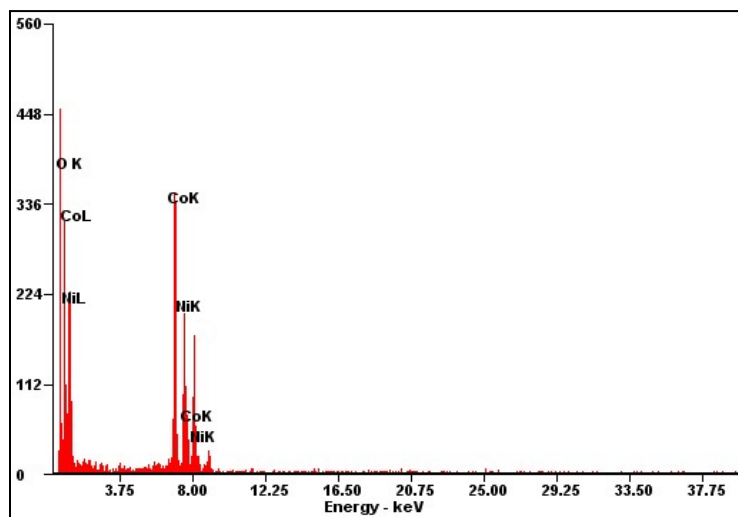
Element	Wt %	At %
O K	21.88	50.74
CoL	40.79	25.67
NiL	36.29	22.93
CoK	00.73	00.46
NiK	00.32	00.20

Figure S3 EDAX profile and **Table S1** representing the related wt/at% of the constituent elements in NCO_HHNB.
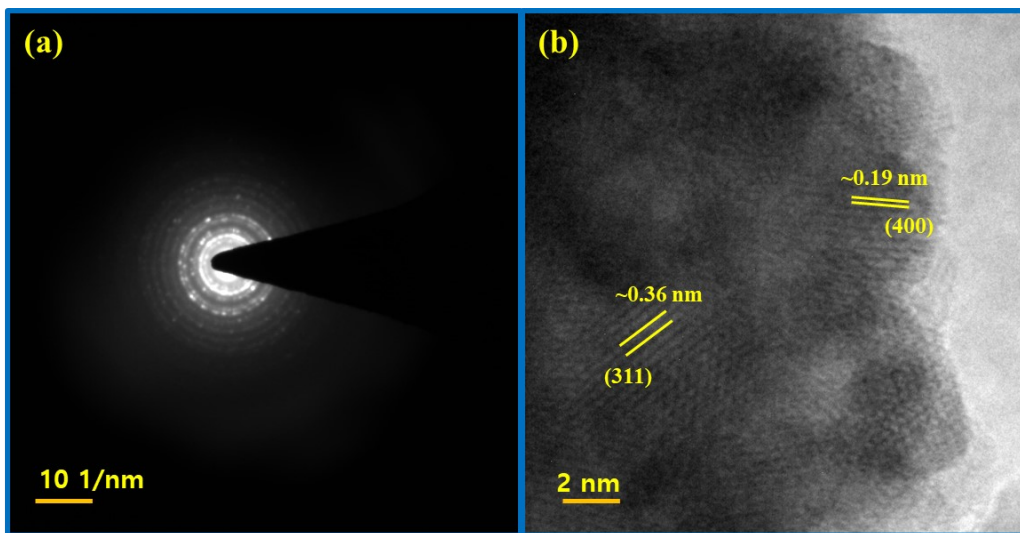
Figure S4(a) Diffraction pattern and (b) fringe pattern for NCO_HHNB.

The crystallographic properties of NCO_HHNB are investigated by SAED. As shown in Fig. S4a, the infused rings of the specified crystallographic planes confirmed the polycrystalline nature of the material. This is actually observed in case of most of the nanostructured materials. However, the rings were still distinguishable and can be matched with the planes discussed in the XRD profile. Fig. S4b showing the fringe pattern provided information about the lattice spacing which was found to be ~0.36 nm (from (311) plane) and ~0.19 nm (from (400) plane). The results proved that the coexistence of Ni and Co keep the spinel structure maintained due to the nearly similar

ionic radii of both the ions. However, it is expected that coexistence of these two different ions to form a single compound may introduce defects in the unit cell structure which thus created oxygen vacancy. This could affect the electrical and electronic property and thus, induce a synergistic enhancement in the electrochemical activity
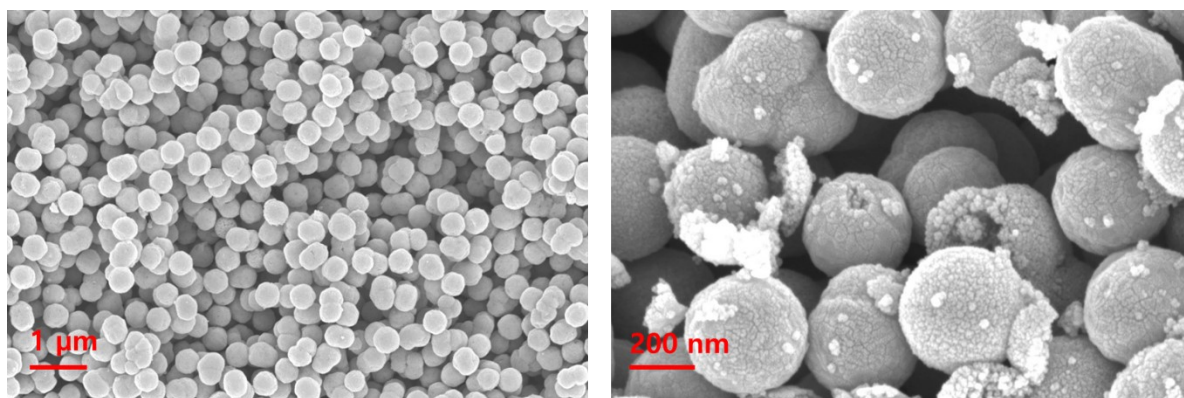

Figure S5 SEM micrographs of NCO_HHNB synthesized in 500 mL reactor.
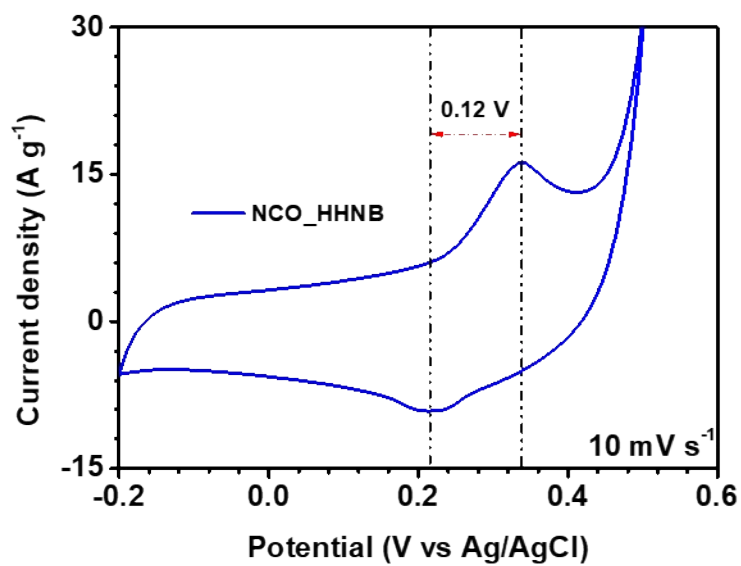
Figure S6 CV profile of NCO_HHNB based electrode in three electrode configuration at 10 mV s^{-1}.
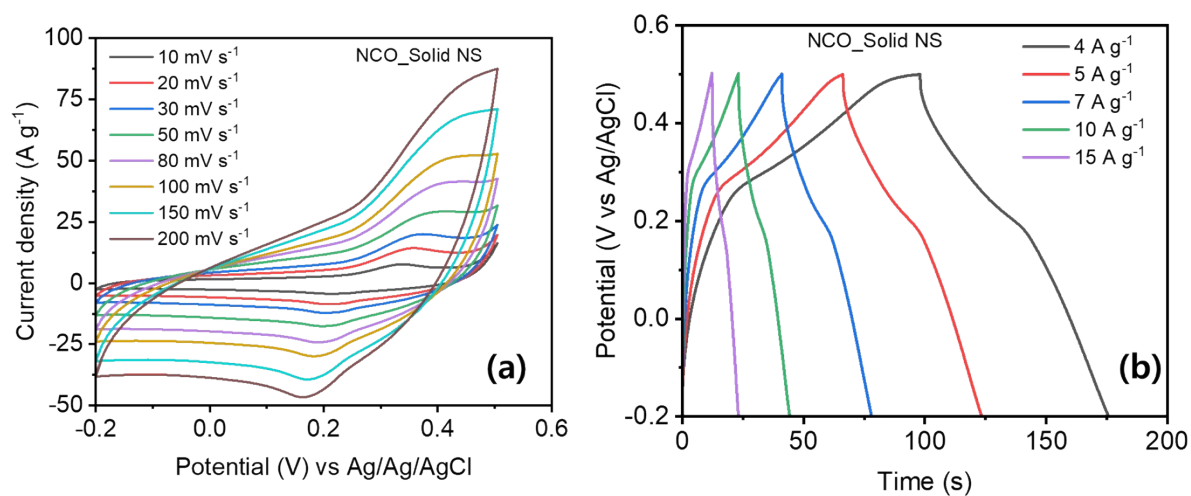

Figure S7 CV and CD profiles of NCO_Solid NS based electrode in three electrode configuration at various scan rates and current densities.
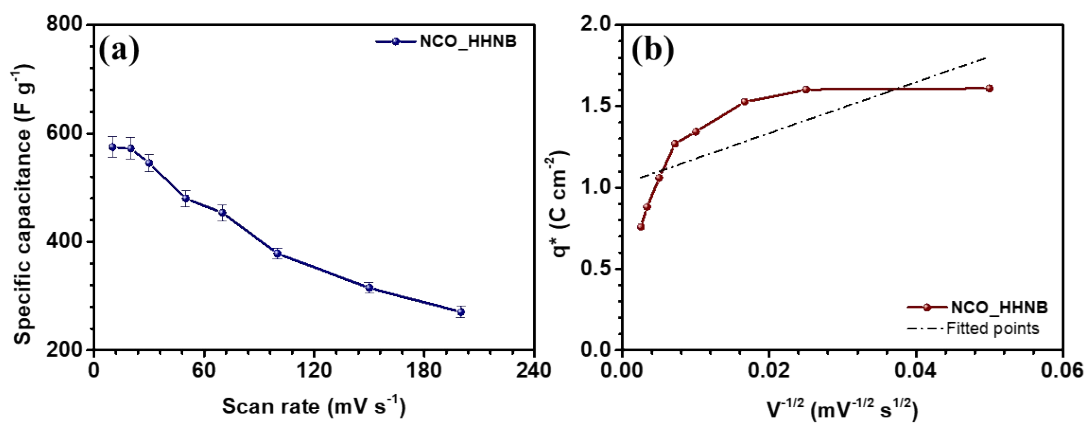
Figure S8(a) Variation of specific capacitance with scan rate and (b) double later charge q_0 variation with inverse square root of scan rate for NCO_HHNB based electrode.
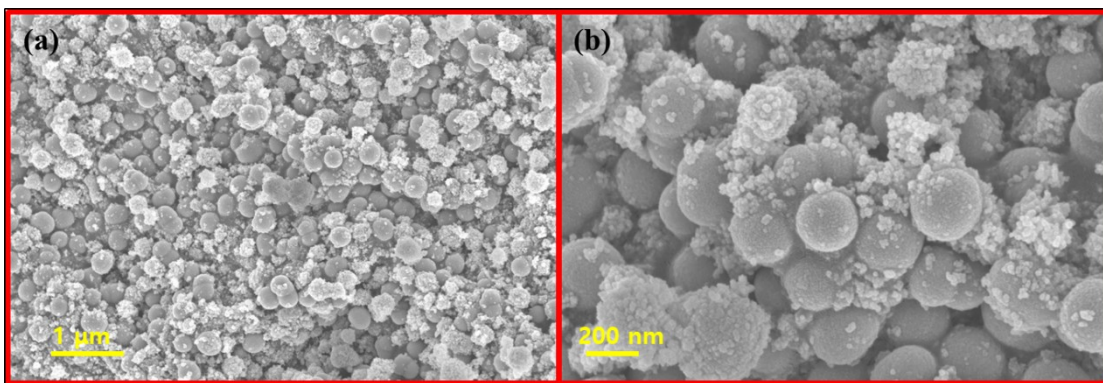
Figure S9 SEM micrographs of electrode material after 6000 cycles.
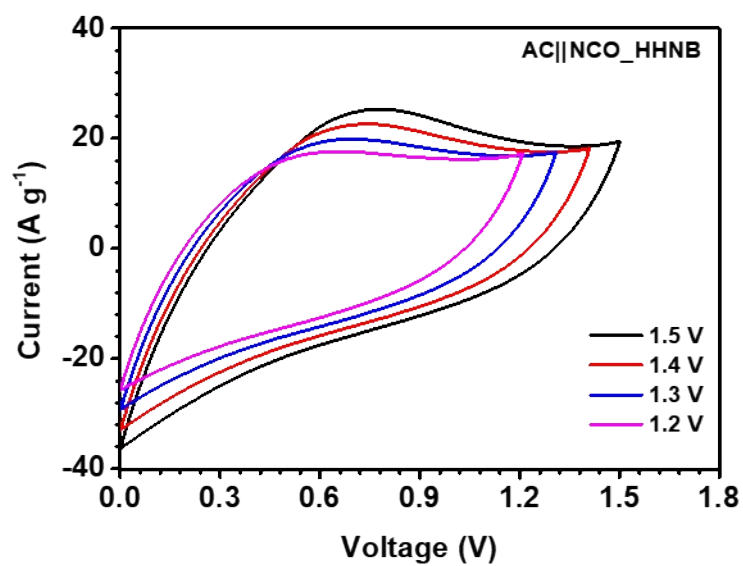
Figure S10 Voltage window optimization for AC‖NCO_HHNB asymmetric supercapacitor.

Scan rate (mV s^{-1})	Specific capacitance (F g^{-1})
10	575
20	572
30	545
50	480
70	453

Table S2 Specific capacitance values at different scan rates for NCO_HHNB electrode.

Current density (A g^{-1})	Specific capacitance (F g^{-1})
100	378
150	315
200	271

Table S3 Specific capacitance values at different current densities for AC||NCO_HHNB asymmetric supercapacitor.

1	127
2	114
3	105
5	97
8	85
10	76

Table S4 Energy and power density values at different current densities for AC||NCO_HHNB asymmetric supercapacitor.

Current density (A g^{-1})	Energy density (Wh kg^{-1})	Power density (W kg^{-1})
1	39.6	767
2	35.6	1577
3	32.8	2408
5	30.3	3942
8	26.5	6622
10	23.7	9873

Table S5 Comparison of present work result with some of the recent results reported in the literature for nearly similar materials.

Electrocatalyst	Methanol concentration (M)	Applied voltage (V)	Onset potential (V)	Current density (mA cm^{-2})	Reference
NiCo$_2$O$_4$/carbon xerogel	0.5	0.6	~0.310	98	[3]
NiCo$_2$O$_4$ nanocloth	0.5	0.6	~0.190	134	[4]
NiCo$_2$O$_4$ nanosheet	0.5	0.6	~0.160	111	[4]
PVP modified ZnCo2O4	0.5	0.6	~0.316	154	[5]
PVP modified NiCo2O4	0.5	0.6	~0.285	280	[5]
NiCo$_2$O$_4$ nanoparticles	0.5	0.6	~0.35	20	[6]
NiCo$_2$O$_4$ nanoflowers	0.5	0.6	~0.32	60	[6]
Co-P nanowall array	0.5	0.5	~0.3	96	[7]
NCO_HHNB	*0.5*	*0.5*	*0.278*	*502*	*Present work*

References

1.   V. Sharma, I. Singh and A. Chandra, *Sci. Rep.*, 2018, **8**, 1307.

2.   J. Balamurugan, T. T. Nguyen, V. Aravindan, N. H. Kim, S. H. Lee and J. H. Lee, *Nano Energy*, 2019, **65**.

3.   M. M. El-Deeb, W. M. A. El Rouby, A. Abdelwahab and A. A. Farghali, *Electrochim. Acta*, 2018, **259**, 77-85.

4.   W. Wang, Q. Chu, Y. Zhang, W. Zhu, X. Wang and X. Liu, *New J. Chem.*, 2015, **39**, 6491-6497.

5.   Gracita M. Tomboc, Medhen W. Abebe, Anteneh F. Baye, Hern Kim, J. Energy Chem., 2019, **29**, 136-146

6.   A. Y. Faid and H. Ismail, *ChemistrySelect*, 2019, **4**, 7896-7903.

7.   D. Liu, W. Lu, K. Wang, G. Du, A. M. Asiri, Q. Lu and X. Sun, *Nanotechnology*, 2016, **27**, 44LT02.